nGnG Amacrine Cells and Brn3b-negative M1 ipRGCs are Specifically Labeled in the ChAT-ChR2-EYFP Mouse

Ling-Jie Cui, Wen-Hao Chen, Ai-Lin Liu, Xu Han, Shi-Xiang Jiang, Fei Yuan, Yong-Mei Zhong, Xiong-Li Yang, and Shi-Jun Weng

State Key Laboratory of Medical Neurobiology and MOE Frontiers Center for Brain Science, Institutes of Brain Science, Department of Neurology and Department of Ophthalmology, Zhongshan Hospital, Fudan University, Shanghai, China

Purpose. Experimental access to specific cell subtypes is essential for deciphering the complexity of retinal networks. Here, we characterized the selective labeling, caused by ectopic transgene expression, of two atypical retinal neurons in the ChAT-Channelrhodopsin-2 (ChR2)-EYFP mouse.

Methods. Retinal sections and flat-mounts were prepared for double-staining immunohistochemistry with antibodies against EYFP and various neuronal markers. Sagittal/coronal brain slices were made to visualize EYFP signals in central nuclei. Whole-cell recordings were conducted to test the functionality of ChR2.

Results. Two populations of EYFP-positive retinal cells were observed. The inner nuclear layer (INL)-located one (type I cell) distributed regularly throughout the entire retina, whereas the ganglion cell layer (GCL)-residing one (type II cell) was restricted ventrally. None of them was cholinergic, as evidenced by the complete absence of ChAT immunoreactivity. Type I cells were immunolabeled by the amacrine marker syntaxin. However, the vast majority of them were neither positive to GABA/GAD65, nor to GlyT1/glycine, suggesting that they were non-GABAergic non-glycinergic amacrine cells (nGnG ACs), which was confirmed by double-labeling with the nGnG AC marker PPP1R17. Type II cells were immunopositive to melanopsin, but not to Brn3a or Brn3b. They possessed dendrites stratifying in the outermost inner plexiform layer (IPL) and axons projecting to the suprachiasmatic nucleus (SCN) rather than the olivary pretectal nucleus (OPN), suggesting that they belonged to a Brn3b-negative subset of M1-type intrinsically photosensitive retinal ganglion cells (ipRGCs). Glutamatergic transmission-independent photocurrents were elicited in EYFP-positive cells, indicating the functional expression of ChR2.

Conclusions. The ChAT-ChR2-EYFP retina exhibits ectopic, but functional, transgene expression in nGnG ACs and SCN-innervating M1 ipRGCs, thus providing an ideal tool to achieve efficient labeling and optogenetic manipulation of these cells.

Keywords: transgenic mouse, retina, nGnG amacrine cell, ipRGC, melanopsin

In a majority of mammals, neurons in the inner retina, in contrast with their outer retinal counterparts, photoreceptors, and horizontal cells, which typically consist of only two to four subtypes, exhibit extreme diversity.[1,2] At least 40 subtypes of ganglion cells (GCs) have recently been identified by physiological recording,[3] morphological analysis,[4] or single-cell RNA sequencing.[5] As for amacrine cells (ACs), the number of subtypes might even be larger than 60.[6–8]

A key challenge for efficiently investigating neurons of such a tremendous variety is to find a way to label defined AC/GC subtypes specifically. In this respect, genetically modified mice with certain inner retinal neurons targeted by either fluorophores or Cre recombinase offer an invaluable tool.[9–11] Furthermore, when microbial opsin-based light-gated channels, such as Channelrhodopsin-2 (ChR2), were introduced into an AC, the microcircuits composed of it and neighboring GCs could be dissected optogenetically with high reliability.[12–14] The VGluT3-Cre/ChR2-YFP mouse, in which a ChR2-YFP construct is targeted to the VGluT3-expressing glutamatergic ACs (GACs), provides a good example. With this mouse, Lee et al. show that these ACs selectively make glycinergic synapses with a special GC subtype ("uniform detector"), whereas synapses between these cells and a variety of other GCs are glutamatergic.[15]

Although this approach has been successfully used for a wide array of ACs and GCs, there are no ideal genetic mice now available that provide highly selective labeling/manipulation for several subtypes of ACs and GCs, including the non-GABAergic non-glycinergic (nGnG) AC, an atypical AC, and the Brn3b-negative M1-type intrinsically photosensitive retinal ganglion cell (ipRGC). The nGnG ACs, unlike the vast majority of ACs, are not positive to biochemical markers probing GABA or glycine,[16,17] and they are late-born, multistratified ones with a narrow dendritic field.[16] Brn3b-negative M1 ipRGCs belong to one of the two subpopulations of M1 ipRGCs, which lack the expression of the

transcription factor Brn3b and project to the suprachiasmatic nucleus (SCN) rather than the olivary pretectal nucleus (OPN), the central target of Brn3b-positive M1 cells.[18]

Here, we report that in the retina of the ChAT-ChR2-EYFP mouse, which was designed to probe central cholinergic neurons,[19] EYFP is not expressed by cholinergic amacrine cells, but ectopically localized to nGnG ACs and Brn3b-negative M1 ipRGCs. Furthermore, as revealed by targeted patch-clamp recording, the ChR2 light-gated channel is functionally expressed in EYFP-positive cells. Therefore, the ChAT-ChR2-EYFP retina provides a promising model for exploring not only functional properties of these two nonclassical cells, but also neuronal interactions within the circuits containing these cells with optogenetic manipulation.

MATERIALS AND METHODS

Animals

ChAT-ChR2-EYFP transgenic mice (B6.Cg-Tg(Chat-COP4*H134R/EYFP)6Gfng/J) on a C57BL/6 genetic background were kindly provided by Prof. Minmin Luo (Tsinghua University, Beijing, China). These mice incorporate a bacterial artificial chromosome (BAC) gene expressing ChR2-EYFP fusion protein under the control of the ChAT promoter.[19] Genotypes were determined by polymerase chain reaction (PCR) analysis of tail DNA samples, as described previously.[19] To maintain a live colony, offsprings were generated by crossing the hemizygous mice with wildtype littermates or C57BL/6JSlac mice (SLAC Laboratory Animal Co., Ltd., Shanghai, China). Adult mice aged 2 to 4 months of either sex were used for experiments. Animals were housed in groups of two to four per cage in a temperature-controlled room under a 12/12 light/dark cycle, with food and water provided ad libitum. All protocols for animal breeding and handling were approved by the Institutional Animal Care and Use Committee of Fudan University and were in accordance to the ARVO Statement for the Use of Animals in Ophthalmic and Vision Research. All efforts were made in order to minimize animal suffering.

Tissue Preparation for Immunohistochemical Experiments

Animals were euthanized by cervical dislocation. Eyes were removed immediately and dissected in 0.01 M phosphate-buffered saline (PBS; pH 7.4). The cornea, lens, and vitreous were removed, leaving the retina in the posterior eyecup. For whole-mounts, the retinas were gently dissected from the eyecup, and four small incisions were made to lay the retina flat. Then, the retinas were mounted ganglion cell side up on a piece of nitrocellulose membrane (AABP04700, Millipore, Billerica, MA, USA) and fixed with 4% paraformaldehyde (PFA) in 0.1 M PBS (pH 7.4) for 30 minutes. For vertical sections, eye cups were fixed in 4% PFA for 20 minutes and then cryoprotected at 4°C in successive solutions of 0.1 M PBS containing 10% (w/v), 20%, and 30% of sucrose. After that, eye cups were embedded and stored at −80 °C in optimal cutting temperature (OCT) medium (Sakura Finetek, Torrance, CA, USA) until being sectioned at 14 to 16 μm using a CM1950 cryostat microtome (Leica Microsystems, Wetzlar, Germany). Pieces of retinas were collected on Super-Frost Plus glass slides (Thermo Fisher Scientific, Waltham, MA, USA) and stored at −20°C. To

TABLE 1. List of the Primary Antibodies Used in This Study

Antibody	Host	Source	Dilution
Brn3a	Goat	Santa Cruz, sc-31984	1:800
Brn3b	Goat	Santa Cruz, sc-6026	1:500
bNOS	Rabbit	Sigma, N7155	1:2000
Calbindin	Mouse	Swant, 300	1:1000
ChAT	Goat	Millipore, ab144p	1:1000
ChR2	Mouse	Progen, 651180	1:1000
Chx10	Sheep	Abcam, ab16141	1:1000
GABA	Guinea pig	Millipore, ab175	1:200
GAD65	Mouse	Abcam, ab26113	1:1000
GFP	Chicken	Aves Labs, 1020	1:1000
Glycine	Rat	David Pow	1:1500
GlyT1	Goat	Chemicon, ab1770	1:10000
Melanopsin	Rabbit	ATS, UF006	1:10000
Melanopsin	Rabbit	Thermo Fisher, PA1-780	1:1000
PPP1R17	Rabbit	Atlas, HPA047819	1:500
Syntaxin	Mouse	Sigma, S0664	1:1000
TH	Mouse	Sigma, T2928	1:10000
VGluT1	Guinea pig	Millipore, ab5905	1:1000
VGluT3	Guinea pig	Millipore, ab5421-1	1:1000
VIP	Rabbit	Immunostar, 20077	1:500

prepare brain sections, animals were anesthetized with 0.6% sodium pentobarbital (200 mg/kg), and perfused transcranially with 0.9% saline followed by cold, freshly prepared 4% PFA. Then, the brains were removed and postfixed overnight in 4% PFA followed by cryoprotection in 30% sucrose in 0.1 M PBS at 4°C. The brains were then frozen and stored at −80°C in OCT medium. Serial 50-μm-thick sagittal or coronal sections were cut using a CM1950 cryostat, collected on Super-Frost Plus slides, and stored at −20°C.

Antibodies

All the primary antibodies (Table 1) used in this study have been characterized in the mammalian retina, and our staining patterns matched those documented in other studies. Alexa Fluor 488/555/647-conjugated fluorescent secondary antibodies were obtained from Thermo Fisher or Jackson ImmunoResearch (West Grove, PA, USA). They were raised in either goat or donkey against the primary antibody's host species, and used with a final dilution typically at 1:200.

Immunohistochemical Staining

Retinal whole-mounts were pretreated with a blocking solution (6% donkey serum, 1% Triton X-100 in 0.1 M PBS) for 2 hours at room temperature, and then incubated with primary antibodies in a buffer solution (3% donkey serum, 1% bovine serum, and 1% Triton X-100 in 0.1 M PBS) for 3 days at 4°C. They were washed (3 × 15 minutes) in 0.1 M PBS, incubated with secondary antibodies overnight at 4°C in the dark, washed again, and mounted onto glass microscope slides, and coverslipped with VECTASHIELD mounting medium (Vector Laboratories, Burlingame, CA, USA). For retina and brain sections, after rinsing in PBS, the sections were pretreated with a blocking solution (6% donkey serum, 0.2% Triton X-100 in 0.1 M PBS) for 2 hours at room temperature to saturate nonspecific binding sites. The sections were incubated overnight at 4°C in primary antibodies diluted in an incubation solution (3% donkey serum, 1% bovine serum, and 0.2% Triton X-100 in 0.1 M PBS), followed by washing three times with PBS, and they were then incubated

with secondary antibodies for 2 hours at room temperature, washed again, and coverslipped with VECTASHIELD.

Image Acquisition and Quantification

Immunofluorescence images (captured at a laser-scanning rate of 12.5 μs/pixel) were acquired with an Olympus FV1000 laser scanning confocal microscope (Olympus Corporation, Tokyo, Japan) equipped with 405, 488, 559, and 635 nm lasers. Confocal scans were conducted using a 20 × (N.A. 0.75) dry, a 40 × (N.A. 0.95) dry, or a 60 × (N.A. 1.42) oil-immersion objective at the resolution of 1024 × 1024 pixels. To avoid crosstalk between channels in double-labeling experiments, images were acquired separately from each laser channel on single-layer optical sections. The brightness and contrast of digital images were adjusted in Photoshop CS5 (Adobe Systems, San Jose, CA, USA) and all adjustments were made uniformly to the entire image.

To reconstruct soma-dendritic profiles, confocal images of individual EYFP-positive cells were collected at 1 μm intervals from multiple optical planes. The confocal stack of the full dendritic field was merged using the maximum-intensity projection function of Photoshop CS5. Soma diameter, dendritic field diameter, primary dendrite number, and branch points were measured by neuronal tracing with Neurolucida software (Microbrightfield, Williston, VT, USA). Soma diameter was calculated as the diameter of a circle, which has the same area as the contour around the cell body. Dendritic field diameter was estimated by calculating the diameter of a circle having the same area as a convex polygon minimally enclosing the dendritic field. Data are reported as mean ± SEM.

For the construction of whole-retina images as shown in Figures 1B, 1C, multiple overlapping images covering the entire retina, focused at either the ganglion cell layer (GCL) or the inner nuclear layer (INL), were collected using a fluorescence microscope (Axioskop 40; Carl Zeiss Inc., Oberkochen, German) with a 40 × lens (N.A. 0.95). Collected images were then assembled into a single photographic montage containing the entire retina using Photoshop CS5. Based on such montages, the total number of EYFP-positive cells in each retina and topographic locations of individual cells were examined manually.

Intraocular Injection

To anterogradely label retinal projections to the SCN and OPN, 1 μL of cholera toxin B (CTB) subunit conjugated with Alexa Fluor 594 (C35777; Thermo Fisher) was delivered into the vitreous body with a pulled glass micropipette (10–30 μm in tip size) using a Nanoject II microinjector (3-000-205/206; Drummond Scientific Company, Broomall, PA, USA). The micropipette was left in place for approximately 1 minute before being slowly retracted. Three to 4 days after injection, the mice were euthanized, and brain slices were prepared as described above.

Electrophysiology

For whole-cell patch-clamp recordings, mice were dark-adapted overnight, and all experimental procedures were performed under very dim red light. Mice were euthanized by sodium pentobarbital (0.6%) overdose, and whole-mount retinal preparation prepared as described previously.[20] The retinal whole-mount was then transferred into a record-ing chamber (RC-26GLP; Warner Instruments, Hamden, CT, USA) and perfused (3−4 mL/min) with carbogen-saturated Ames' medium (A1420; Sigma, St. Louis, MO, USA) at 32 to 34°C. EYFP-positive cells in the INL were identified by epifluorescence evoked by a C-FL-C GFP-B filter set (Nikon Instruments Inc., Melville, NY, USA) and viewed by an upright microscope (FN-1, Nikon) equipped with a 40 × water immersion objective (N.A. 0.8) and a CMOS camera (opti-MOS; QIMAGING, Surrey, Canada). Voltage-clamp recordings were performed with pipettes (tip resistance 5–7 MΩ) containing (in mM): 120 Cs-methanesulfonate, 5 TEA-Cl, 10 HEPES, 10 BAPTA, 3 NaCl, 2 QX-314-Cl, 4 ATP-Mg, 0.4 GTP-Na, and 10 phosphocreatine-Tris, adjusted to pH7.2, 280 mOsm. Signals were amplified with a MultiClamp 700B amplifier (Molecular Devices, Sunnyvale, CA, USA), low-pass filtered at 2.4 kHz, and sampled at 10 kHz with a Digidata 1550 A/D converter (Molecular Devices). Inward photocurrents were recorded at the holding potential near the reversal potential for Cl^- (-67 mV), after correcting for the liquid junction potential of -10 mV. Series resistance, typically <40 MΩ, was compensated by 50%. Full-field light stimuli at 2.7×10^{16} photons·cm^{-2}·s^{-1} were generated by an LED illuminator (X-cite 110LED; Excelitas Technologies, Waltham, MA, USA), band-pass filtered at 470 ± 20 nm with the GFP-B fluorescent filter set, and presented through the objective lens. To block glutamatergic transmission so that optogenetic responses could be isolated, L-AP4 (50 μM), DNQX (40 μM), ACET (2 μM), and D-AP5 (30 μM), purchased from either Tocris Biosciences (Ellisville, MO, USA) or Sigma, were included in Ames' medium.

RESULTS

General Cellular Labeling Pattern in the ChAT-ChR2-EYFP Retina

We first examined the general profile of transgene expression in whole-mount retinas harvested from ChAT-ChR2-EYFP mice. To enhance the visibility of EYFP fluorescence, an antibody recognizing EYFP was used, and this strategy was applied throughout this study. Figure 1A is a representative microphotograph derived from stacked confocal images, showing a sparse array of retinal cells marked by EYFP. These EYFP-positive cells can be classified into two populations with distinct morphology. One population exhibited small, axonless somata (typically 7 to 8 μm in diameter) and tiny, bushy dendrites, denoted "type I cells", here (white arrowheads), whereas the other population, termed "type II cells", had relatively larger, axon-bearing cell bodies (typically 12–15 μm in diameter), and wide, sparsely branching dendritic fields (white arrows). It was noteworthy that neither of them resembled the well-known cholinergic "starburst" amacrine cells (SACs) morphologically.[21]

To get a precise idea of the number and topographic distribution of the two EYFP-positive cell populations, a few of ChAT-ChR2-EYFP retinas were fully mapped by constructing a photographic montage covering all EYFP cells in each retina (Figs. 1B–D). Type I cells were regularly spaced across all four retinal quadrants. A complete count of these cells yielded 202 ± 36 (n = 5 retinas). The distribution of type II cells, by contrast, was topographically dependent, being confined in the ventral part of the retina. They were significantly outnumbered (81 ± 6 cells per retina, n = 6 retinas) by type I cells (P = 0.027, unpaired *t*-test).
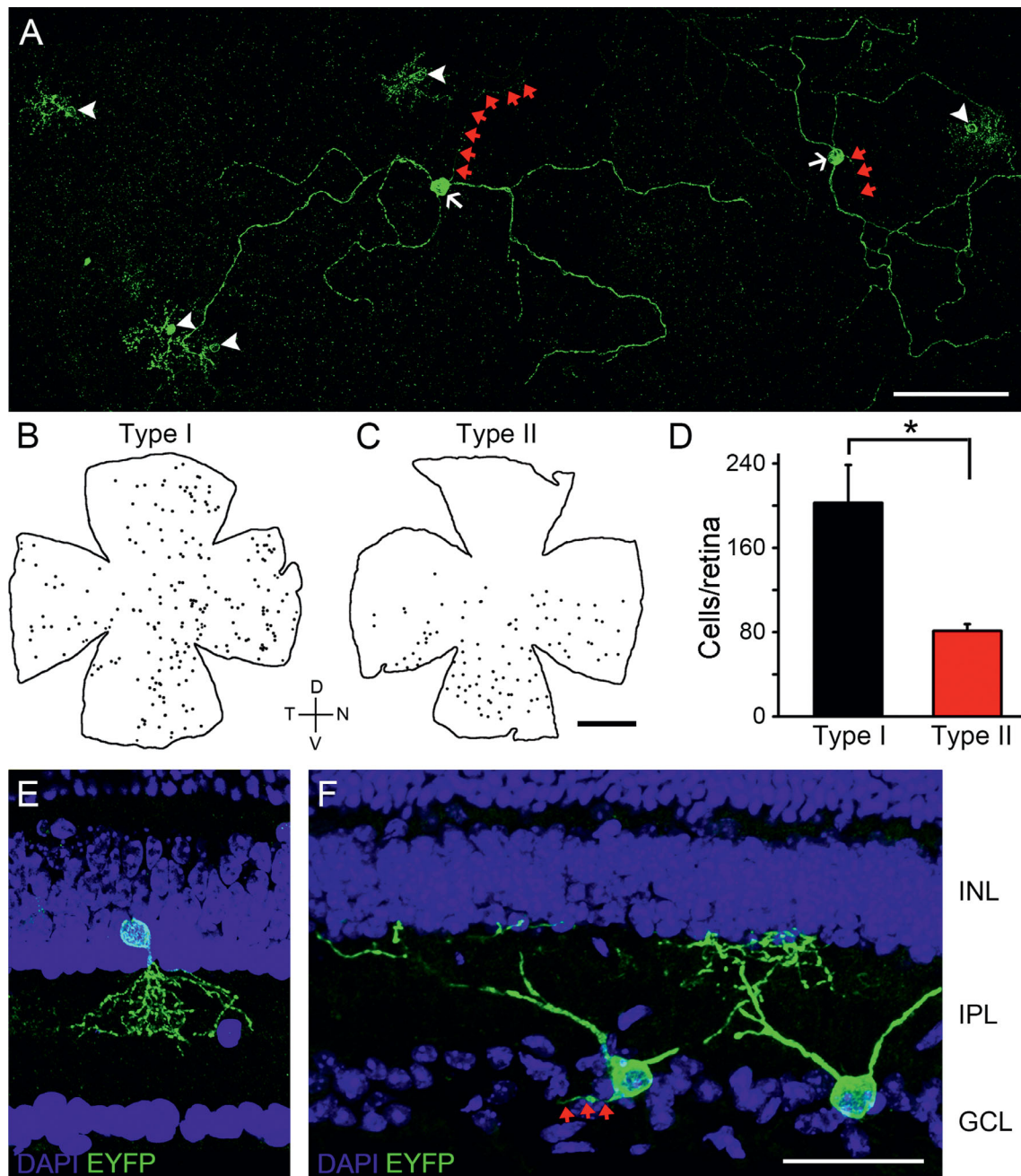
FIGURE 1. **General expression profile of the transgene in the ChAT-ChR2-EYFP retina.** (A) Micrograph of a whole-mount ChAT-ChR2-EYFP retina labeled with an antibody directed to EYFP, which reveals EYFP expression in two cell populations with distinct morphologies: type I cells (white arrowheads) with small somata and narrow, heavily branched dendritic fields and type II cells (white arrows) with large cell bodies and wide-field, sparely branched dendrites. Red arrows point to vaguely labeled axons. Scale bar = 90 μm. (B, C) Representative silhouettes showing topographic distributions of type I (B) and II (C) cells. Scale bar = 1 mm. D, dorsal; V, ventral; T, temporal; N, nasal. (D) Bar chart summarizing the average number of types I and II cells per retina. Error bars represent 1 SEM. (E, F) Representative confocal fluorescence microphotographs of retinal vertical sections, showing the localization of somata and dendrites of a type I (E) and two type II (F) cells. Nuclei were counterstained with DAPI (blue). The type I cell has a soma located in the proximal INL and processes arborizing diffusely across the sublaminae S1-S3 of the IPL. The type II cells have somata located in the GCL and processes ramifying at the outermost IPL. An axon can be seen (red arrows). Scale bar = 40 μm.

Frozen retinal section preparations revealed that the somata of type I cells were restricted to the proximal half of the INL, a region where AC somata are localized (Fig. 1E). Their small dendritic arbors ramified diffusely across the distal part (approximately S1 to S3) of the inner plexiform layer (IPL). All these morphological characteristics of type I cells suggest that they might belong to multistratified narrow-field ACs. On the other hand, the somata of type II cells resided exclusively in the GCL, with their dendrites being sharply monostratified, and projecting to the outermost region of the IPL (Fig. 1F). These morphological features resembled those of OFF-type GCs.

TABLE 2. Statistics for Co-localization of EYFP-positive Cells with Various Molecular Markers

Soma Location	Cell Marker	# of EYFP+ Cells Counted	# of Marker-labeled EYFP+ Cells (%)	# of Retinas or Brains
INL	ChAT	86	0 (0%)	6
	Calbindin	76	0 (0%)	6
	Chx10	112	0 (0%)	6
	Syntaxin	115	115 (100%)	7
	Brn3a	71	0 (0%)	4
	GABA	65	1 (1.54%)	4
	GAD65	68	0 (0%)	7
	GlyT1	118	3 (2.54%)	8
	Glycine	107	10 (9.35%)	5
	PPP1R17	134	134 (100%)	7
	TH	91	0 (0%)	4
	VIP	101	0 (0%)	6
	bNOS	98	0 (0%)	6
	VGluT3	114	0 (0%)	6
	VGluT1	55	0 (0%)	4
	ChR2	43	100 (0%)	8
GCL	ChAT	117	0 (0%)	6
	Brn3a	159	0 (0%)	8
	UF006	141	141 (100%)	5
	PA1-780	127	127 (100%)	5
	Brn3b	102	0 (0%)	7
	ChR2	46	100 (0%)	8
Cortex	ChAT	101	98 (97.03%)	5
Striatum	ChAT	73	71 (97.26%)	5
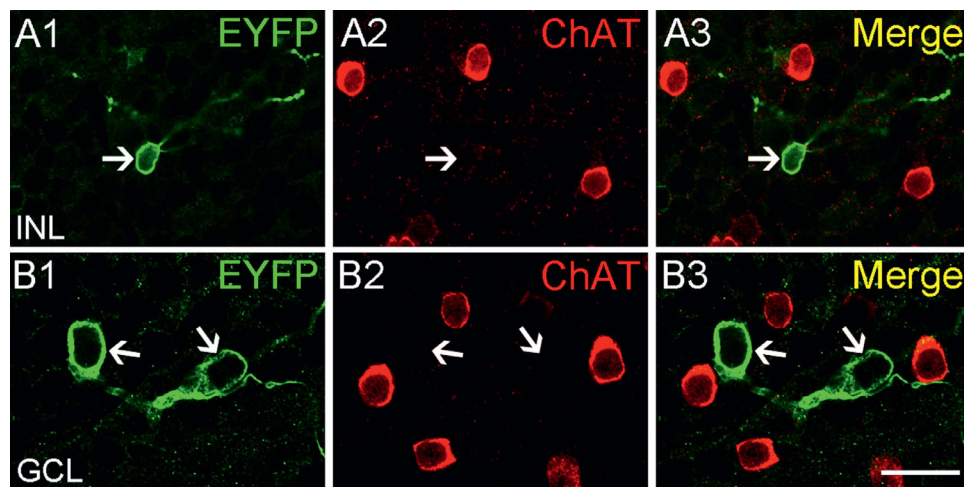
FIGURE 2. Lack of ChAT immunoreactivity in EYFP-positive retinal cells. (A1−B3) Representative micrographs captured from whole-mount retinas double-labeled for EYFP (left panels) and ChAT (middle panels). ChAT labeling is not seen in EYFP-positive neurons in either the INL (A1−A3, type I cells) or GCL (B1−B3, type II cells). Arrows indicate EYFP-labeled, but ChAT-negative cells. Scale bar = 20 μm.

Lack of EYFP Expression in Retinal Cholinergic Neurons

Using a series of biomarkers for specific subtypes of retinal neurons, we sought to determine the identities of both the EYFP-expressing cells, and the quantitative results are summarized in Table 2.

Based on the morphological features of EYFP-positive cells, we speculated that transgene expression pattern may exhibit an "ectopic" mode in the ChAT-ChR2-EYFP retina. This speculation was explored by double-labeling with EYFP and ChAT (a specific marker for cholinergic ACs) in retinal whole-mounts. As shown in Figure 2, neither type I (0%, 0 of 86 cells collected from 6 retinas) nor type 2 EYFP cells (0%, 0 of 117 cells collected from 6 retinas) showed detectable ChAT immunoreactivity. In contrast, strong EYFP expression was seen in various brain areas known to contain abundant cholinergic neurons, including cortex, striatum, basal forebrain, etc. (Supplementary Fig. S1A), with a pattern rather comparable to that reported previously in this mouse.[19] Furthermore, double-staining immunohistochemistry showed that the vast majority of central EYFP-positive neurons were immunoreactive to ChAT (cortex: 97.03%, 98 of 101 cells collected from 5 brains, Supplementary Figs. S1B1−B3; striatum: 97.26%, 71 of 73 cells collected from 5 brains, Supplementary Figs. S1C1−C3) in this mouse. Thus, the ectopic expression of ChR2-EYFP transgene construct seemed to be retina-specific.
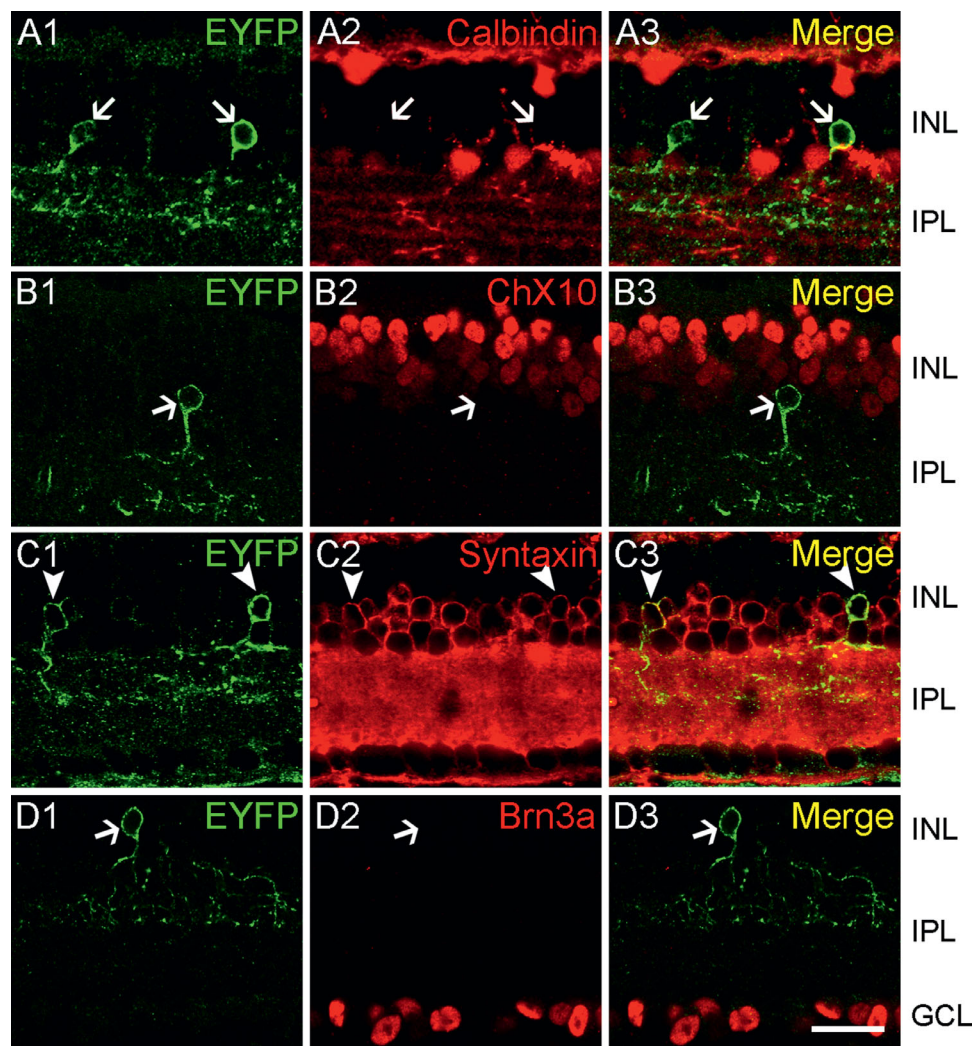
FIGURE 3. EYFP immunoreactivity in the INL is localized to amacrine cells. EYFP-expressing retinal sections were immunostained for the horizontal cell marker calbindin (**A1−A3**), bipolar cell marker Chx10 (**B1−B3**), amacrine cell marker syntaxin (**C1−C3**) and ganglion cell marker Brn3a (**D1−D3**). As observed in the merged images (right panels), EYFP-positive cells lack any detectable immunoreactivity for calbindin, Chx10, or Brn3a (arrows), but are immunopositive to syntaxin (arrowheads). Scale bar = 20 μm.

INL-residing ChR2-EYFP-positive Neurons are nGnG Amacrine Cells

Double-labeling experiments conducted in vertical sections found that type I EYFP-positive cells were not stained by the horizontal cell marker calbindin (0%, 0 of 76 cells collected from 6 retinas, Figs. 3A1–A3), or by the bipolar cell marker Chx10 (0%, 0 of 112 cells collected from 6 retinas, Figs. 3B1–B3). Instead, all of EYFP-positive cells examined were found to exhibit the immunoreactivity of syntaxin (also known as HPC-1), an AC marker (115 of 115 cells collected from 7 retinas; Figs. 3C1–C3). Moreover, type I cells were unlikely displaced GCs, because they were axonless and not immunopositive to Brn3a (0%, 0 of 71 cells collected from 4 retinas, Figs. 3D1–D3), a GC marker known to label a large fraction (approximately 80−90%) of rodent GCs.[22,23] Together, these findings indicated that they were ACs.

Double-labeling experiments further demonstrated that almost none of these cells was labeled by the GABAergic neuron markers GABA (1.54%, 1 of 65 cells collected from 4 retinas, Figs. 4A1–A3) and glutamic acid decarboxylase

(GAD) 65 (0%, 0 of 68 cells collected from 7 retinas, Figs. 4B1–B3). Meanwhile, only a very limited number of them were immunopositive to the glycinergic neuron markers glycine transporter (GlyT) 1 (2.54%, 3 of 118 cells collected from 8 retinas, Figs. 4C1–C3) and glycine (9.35%, 10 of 107 cells collected from 5 retinas, Figs. 4D1–D3). These results indicated that most, if not all, of type I cells belonged to an atypical "nGnG" amacrine subgroup.[16]

Recently, a specific nGnG AC marker (PPP1R17) has been identified.[24,25] Double-labeling experiments with antibodies directed to EYFP and PPP1R17 were carried out on vertical sections. All of the 134 EYFP-positive type I cells examined (collected from 7 retinas) were co-labeled by PPP1R17 (Figs. 4E1–E3). By contrast, none of type I cells examined were labeled by any of the other four well-defined markers (TH, VIP, bNOS, and VGluT3) recognizing specific AC subtypes (Figs. 5A1–D3 and Table 1). In addition to the lack of VGluT3 immunoreactivity, type I cells were also negative to VGluT1 (Figs. 5E1–E3 and Table 1), confirming that they did not use glutamate as a transmitter, thus not being GCs. Moreover, the soma-dendritic

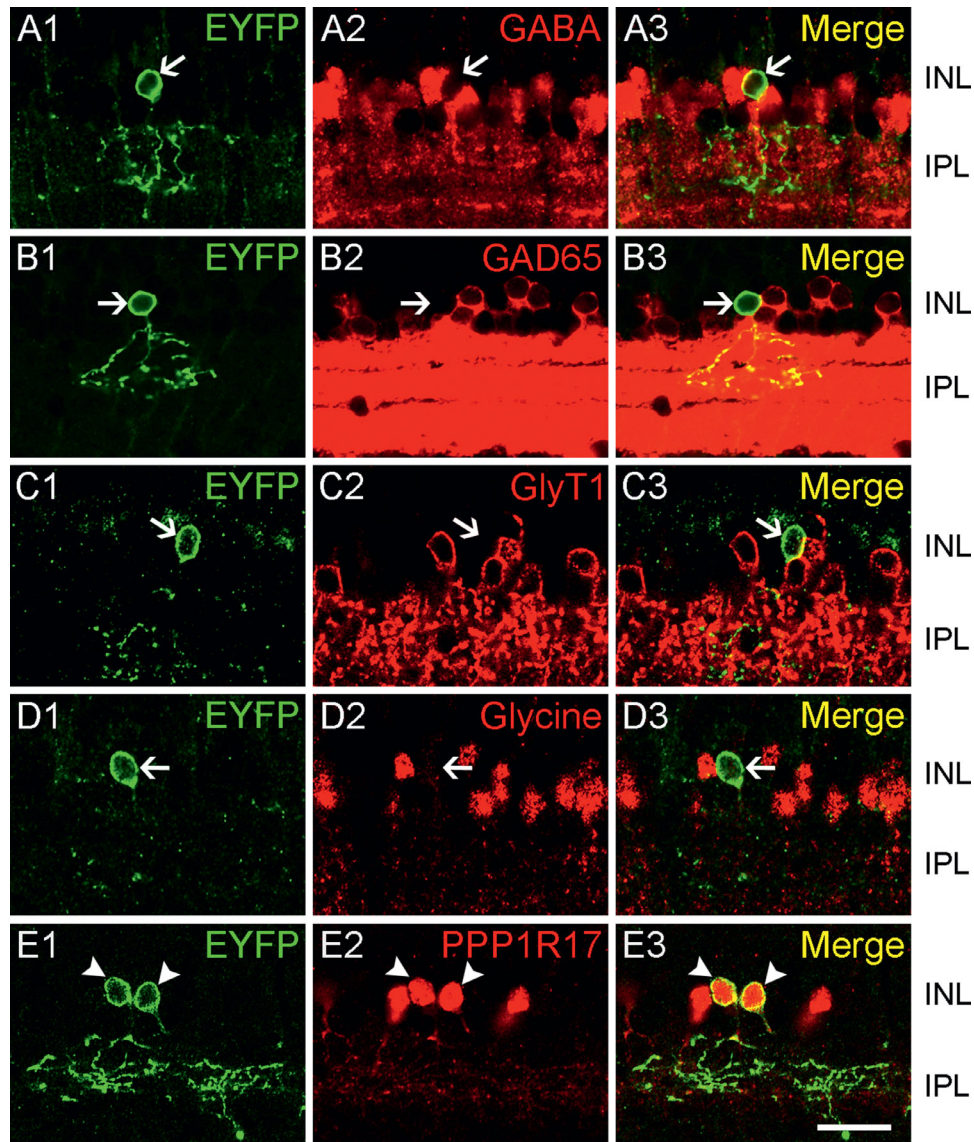**FIGURE 4.** **EYFP immunoreactivity in the INL is localized to nGnG amacrine cells but not to GABAergic or glycinergic amacrine cells.** Retinal sections were co-stained with EYFP and biomarkers for three major classes of ACs, including: GABAergic makers GABA (**A1−A3**) and GAD65 (**B1−B3**), glycinergic markers GlyT1 (**C1−C3**), and glycine (**D1−D3**), and PPP1R17, a specific marker for nGnG ACs (**E1−E3**). From the merged images (right panels), it is clear that virtually no immunosignals for GABAergic or glycinergic markers are seen in EYFP-positive cells (arrows) in the INL. By contrast, all EYFP-positive cells exhibit robust PPP1R17 immunoreactivity (arrowheads). Scale bar = 20 µm.

profiles of type I cells revealed in this work, including tiny somata, narrow dendritic fields, and diffusely stratified dendritic arbors across sublaminae S1 to S3 (Fig. 1), were all highly in line with those of nGnG amacrines.[16] We, thus, concluded that type I cells, at least most of them, were nGnG ACs.

EYFP Cells in the GCL Belong to a Subset of M1 ipRGCs Selectively Innervating the SCN

The axon-bearing feature and large, GCL-residing somata strongly suggest that type II cells were most likely GCs. Surprisingly, in a total of 159 of type II cells collected from 8 retinas, none were immunolabeled by the GC marker Brn3a (Figs. 6A1–A3). Since a few subsets of ipRGCs are known to

lack Brn3a immunoreactivity,[26,27] we speculated that type II cells might be ipRGCs. This was later verified by the strong immunostaining of type II cells in response to the melanopsin antibody UF006 (100%, 141 of 141 cells collected from 5 retinas, Figs. 6B1–B3), which probes multiple ipRGC subtypes.[28] In addition, all type II cells could be stained by another less-sensitive melanopsin antibody (100%, 127 of 127 cells collected from 5 retinas, Figs. 6C1–C3), PA1-780, which preferentially labels M1 ipRGCs rather than other ipRGC subtypes in rodents.[29–31] Meanwhile, the reconstruction of randomly selected, individual type II cells from stacked confocal images by Neurolucida (Fig. 6D) revealed that the soma-dendritic profiles of these cells (soma diameter = 13.4 ± 0.5 µm; dendritic field diameter = 230.6 ± 15.3 µm; primary dendrite number = 2.4 ± 0.2; total branch point = 8.4 ± 0.7; n = 11) were consistent with
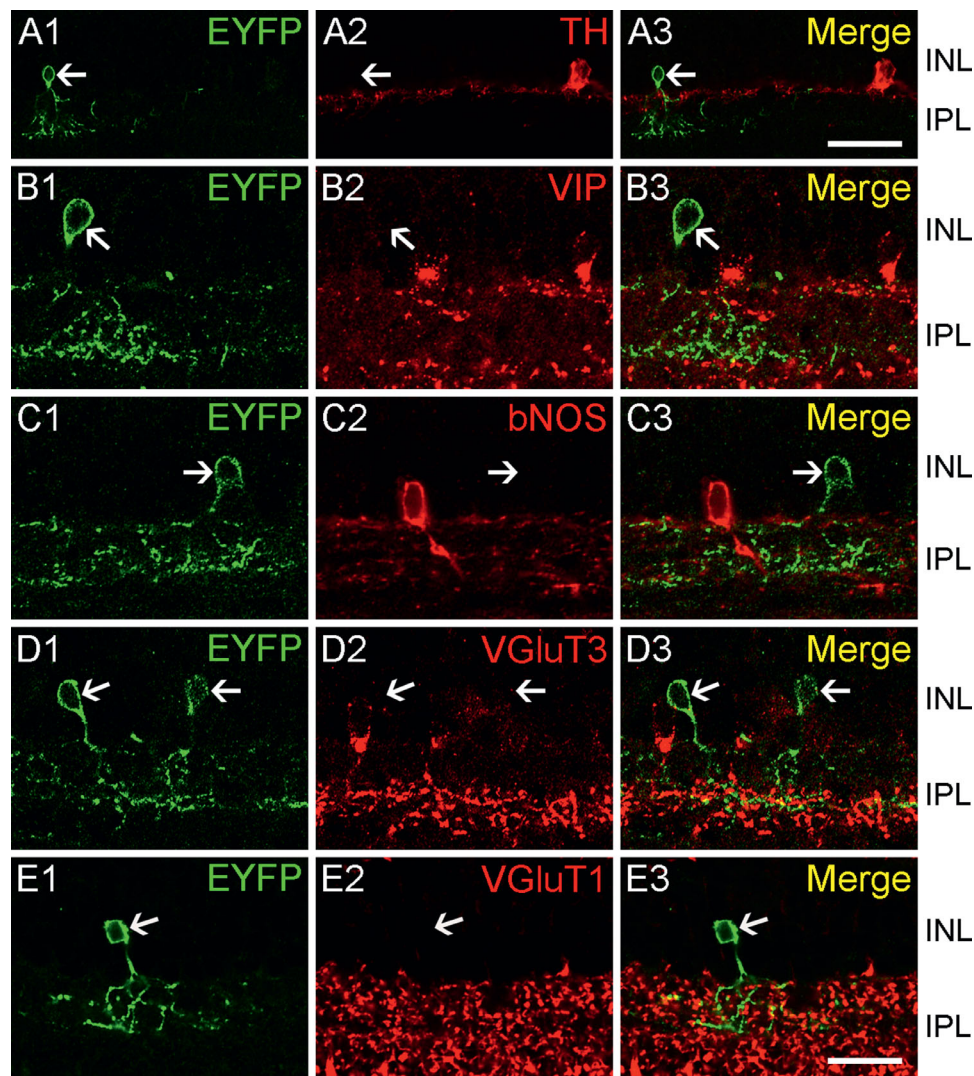
FIGURE 5. Absence of immunoreactivity for various conventional amacrine markers in EYFP-positive INL cells. Vertical sections prepared from ChAT-ChR2-EYFP retinas were co-immunolabeled with antibodies probing EYFP and TH (dopaminergic AC marker, **A1–A3**), VIP (VIP-expressing AC marker, **B1–B3**), bNOS (bNOS-expressing AC marker, **C1–C3**), VGluT3 (glutamatergic AC marker, **D1–D3**), and VGluT1 (glutamatergic neuronal marker, **E1–E3**). Note that virtually no EYFP-positive INL cells are co-labeled by any of the markers listed above. In all the panels, arrows point to EYFP-positive cells, and all these cells were negative to markers listed. TH, tyrosine hydroxylase; VIP, vasoactive intestinal polypeptide; bNOS, nitric oxide synthase, brain (251–270); VGluT3, vesicular glutamate transporter 3; VGluT1, vesicular glutamate transporter 1. Scale bars = 40 μm in **A3** (applies to **A1–A3**) and 20 μm in **E3** (applies to **B1–E3**).

those typical of M1 cells.[28,32,33] Collectively, these results indicated that type II cells were most likely M1-type ipRGCs.

M1 cells could be either Brn3b-positive or -negative. There is evidence that Brn3b-negative ones innervate the SCN, and Brn3b-positive ones project to the OPN.[18] None of type II cells examined were stained by the antibody against Brn3b (0 of 102 cells collected from 7 retinas; Figs. 7A1–A3), indicating that these cells were Brn3b-negative. Indeed, as expected, by tracing central targets of type II cells, it was further demonstrated that densely labeled EYFP-positive fibers were visualized in the SCN (Figs. 7B1–B3), a nucleus known to have a very limited amount of cholinergic innervations,[34,35] but not in the OPN (Figs. 7C1–C3), when these nuclei were anterogradely labeled by intravitreal injection of Alexa Fluor 594-conjugated CTB. These findings strongly suggest that type II cells were among a subset of Brn3b-negative M1 ipRGCs that selectively project to the SCN.

Functional Expression of ChR2

To confirm that ChR2 was indeed co-expressed with EYFP in the retina, just like that reported in central nuclei in this mouse,[19] retinal sections were stained with an antibody directed against ChR2.[36] In all EYFP-positive cells examined, including 43 type I and 46 type II cells, collected from 8 retinas, co-localization of EYFP and ChR2 signals was invariably seen (Figs. 8A1–B3 and Table 2), suggesting the intactness of the ChR2-EYFP fusion protein in spite of the unpredicted, ectopic nature of transgene expression.

Finally, to test whether the expression of ChR2 was truly functional, whole-cell voltage-clamp recordings were performed from EYFP-positive cell bodies in whole-mount retinal preparations (Figs. 8C1 and C2), in which synaptic inputs from rods/cones were silenced by a cocktail blocking glutamatergic transmission (see "Materials and Methods").
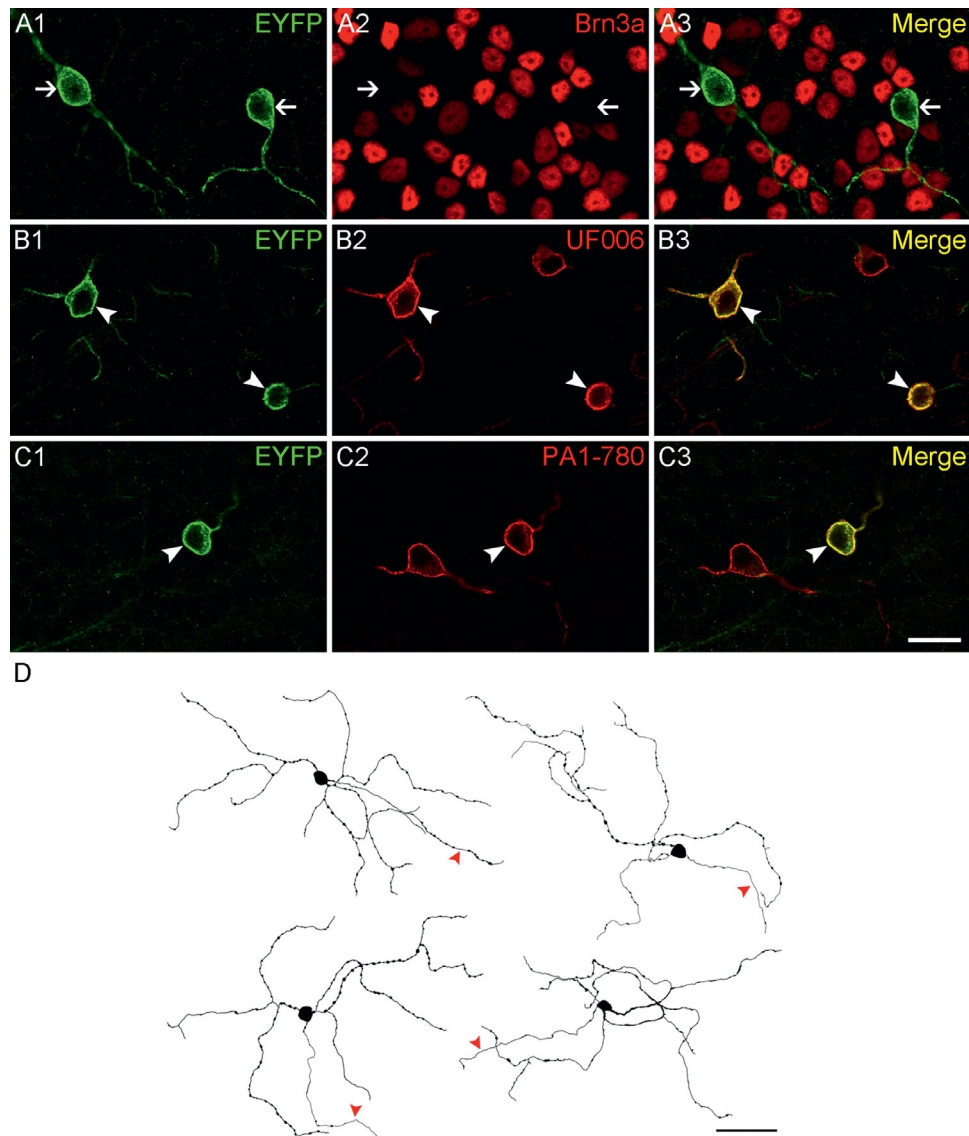
Investigative Ophthalmology & Visual Science

FIGURE 6. EYFP immunoreactivity in the GCL is localized to M1 ipRGCs. (**A1−C3**) Representative micrographs of retinal whole-mounts showing that EYFP-positive somata residing in the GCL lack immunoreactivity of Brn3a (GC marker, arrows in **A1−A3**), but are stained by two melanopsin antibodies, UF006 (marker of various ipRGC subtypes, arrowheads in **B1−B3**) and PA1-780 (M1-type ipRGC marker, arrowheads in **C1−C3**). Scale bar = 20 μm. (**D**) Examples demonstrating the morphological profiles of EYFP-positive GCs as reconstructed from whole-mount retinas. The large, sparsely branched dendritic field is similar among these cells, typical of M1-type ipRGCs. Arrowheads indicate axons. Scale bar = 60 μm.

Because type II cells were melanopsin-expressing, all the recordings were made from type I cells. Inward photocurrents could be evoked by full-field 470 nm light stimulus at 2.7×10^{16} photons·cm^{-2}·s^{-1}, an intensity that exceeds the threshold for ChR2 activation[37] and is commonly used for optogenetic manipulation[38] (Fig. 8C3). Such glutamatergic cocktail-resistant photocurrents reached a peak amplitude (approximately 60 pA) almost immediately after light onset, followed by a current plateau during light stimulation. These features were reminiscent of response kinetics of ChR2 activation, as reported previously.[20,39] Similar results were obtained in all four type I cells (from 4 retinas) examined. Thus, the ChAT-ChR2-EYFP retina possessed well functional ChR2 light-gated channels and could be used for optogenetic manipulation of specific retinal neurons.

DISCUSSION

Ectopic Expression of the ChR2-EYFP Construct

The ChAT-ChR2-EYFP mouse was generated with an original purpose to aid in the studies of cholinergic systems. Indeed, this mouse has proved useful in labeling and manipulating cholinergic neurons in both basal forebrain[40,41] and habenula.[42,43] However, in ChAT-ChR2-EYFP retinas, instead of the cholinergic SACs, nGnG ACs and M1 ipRGCs were found to be EYFP-positive.

Tissue- or nucleus-specific ectopic transgene expression is a common feature observed in transgenic animals.[44,45] In particular, there is a growing body of evidence demonstrating the mismatch between the expression pattern of a transgene and that of the endogenous protein in the
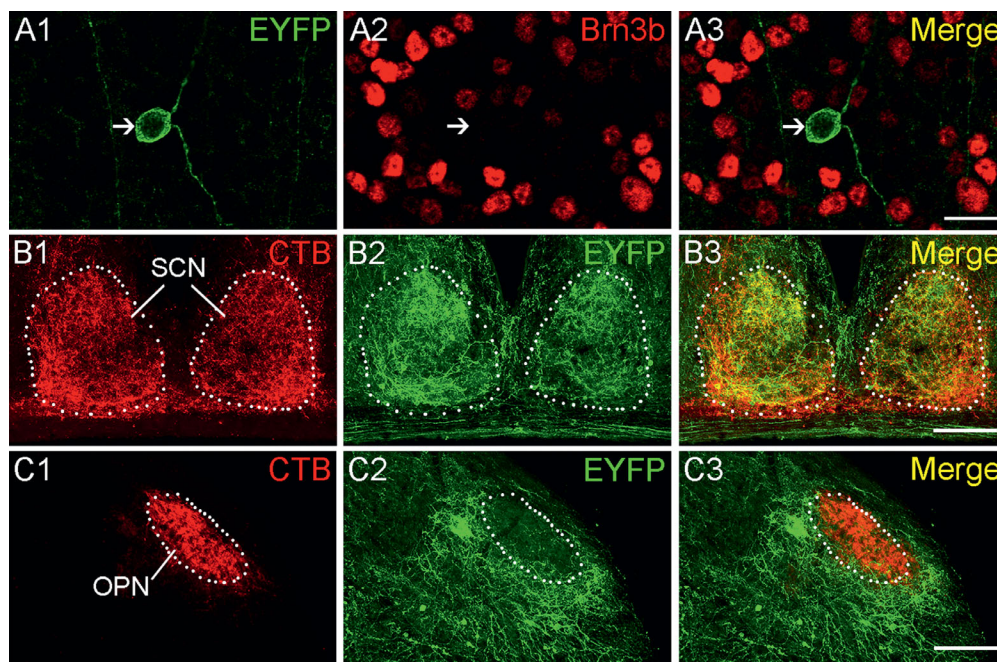
FIGURE 7. Axonal terminations of EYFP-positive M1 ipRGCs in the SCN of the hypothalamus. (**A1−A3**) Representative micrographs of a retinal whole-mount double-stained for EYFP (left) and Brn3b (middle), showing that a GCL-residing EYFP-positive cell (arrow) is Brn3b-negative (right). Scale bar = 20 μm. (**B1−C3**) Coronal brain sections in which retinal projections were labeled by intraocular injection of Alexa Fluor 594-conjugated CTB. Outlines of the SCN and OPN, two NIF visual centers known to receive extensive innervations from M1 ipRGCs, are depicted with white dots. EYFP-positive fibers are enriched in the SCN (**B1−B3**), whereas very few, if any, EYFP signals are observed in the OPN (**C1−C3**). Scale bar = 125 μm.

retina.[9,46–52] It is noteworthy that at least three other ChAT promoter-driven mouse lines (ChAT-Cre/Gsat,[9] ChAT-tauGFP,[52] and ChAT-EGFP[49]) have been reported to exhibit ectopic expressions in the retina. Such ectopic expressions might be caused by various reasons, including transient expression of particular genes during development,[53,54] absence of certain regulatory elements,[45,55] random integration into the genome,[44] and positional influence of the exogenous DNA.[53] Therefore, it is necessary to carefully characterize the retinal expression pattern of any new transgenic animals, especially those under the control of the ChAT promoter, before they are used in retinal research.

Given that the number of ACs in the mouse retina is around 700,000 per retina,[56] and nGnG ACs account for 15% of all ACs,[16] the total number of nGnG ACs should be around 100,000. However, ChR2-EYFP was apparently present only in 200 nGnG ACs (0.2%). In contrast, among all Brn3b-negative M1 cells, which is estimated to be approximately 200,[18,57] 80 cells (40%) were co-labeled by ChR2-EYFP. The fraction displaying ectopic EYFP expression was seemingly cell type-dependent. Fractional labeling of certain cell populations is quite common for ectopic transgene expression. For example, in a TH-tdTomato mouse line that was initially generated for probing dopaminergic neurons, it was found that a small minority of the entire SAC population, which is cholinergic but not dopaminergic, express tdTomato fluorescence.[51]

Specific Labeling of nGnG ACs

An unexpected new finding of the present study is that ChR2-EYFP is quite specifically expressed in nGnG ACs

despite the ectopic nature of such expression. Although the existence of a "third" AC class that is neither GABAergic nor glycinergic has been implicated in the last few decades,[17,58–60] it is until recently that a limited number of molecular markers and genetic mice are available for probing nGnG ACs. Neurod6, a basic helix-loop-helix (bHLH) family transcription factor acting postmitotically to determine the fate of nGnG ACs, is by far the most specific nGnG AC biomarker. However, Neurod6 is likely to be transiently expressed by a second group of ACs (the "SEG" ACs) and other retinal cells at early postnatal stage.[16] Therefore, in the retina of the Nd6CY mouse, obtained by mating the *Neurod6cre* mouse with an YFP reporter line, YFP expression is seen not only in nGnG ACs but also in several non-nGnG AC cells.[16] In another transgenic mouse line named MP (*Thy1-mitoCFP-P*), 98% of CFP-positive ACs are nGnG ACs, but a large number of BCs are also labeled.[16] Because multiple INL neurons are labeled, neither the Nd6CY nor the MP mouse provides an excellent tool for targeting nGnG ACs with high efficiency.

Only two subsets of differentially located cells are labeled in the ChAT-ChR2-EYFP retina, and they could be easily discriminated by distinct morphologies. It should be emphasized that virtually none of the approximately 200 EYFP-expressing ACs in the ChAT-ChR2-EYFP retina were immunoreactive to the GABAergic markers. In addition, over 90% of these cells were not stained by glycine (Fig. 4). These results indicate that the labeling was very specific to nGnG ACs. As for those 9.35% glycine-positive EYFP ACs, it was unlikely that they were functionally glycinergic, since almost none of these cells express GlyT1 (Fig. 4), a key transporter for maintaining normal functions of glycinergic neurons. It is, therefore, safe to say that the ChAT-ChR2-EYFP mouse
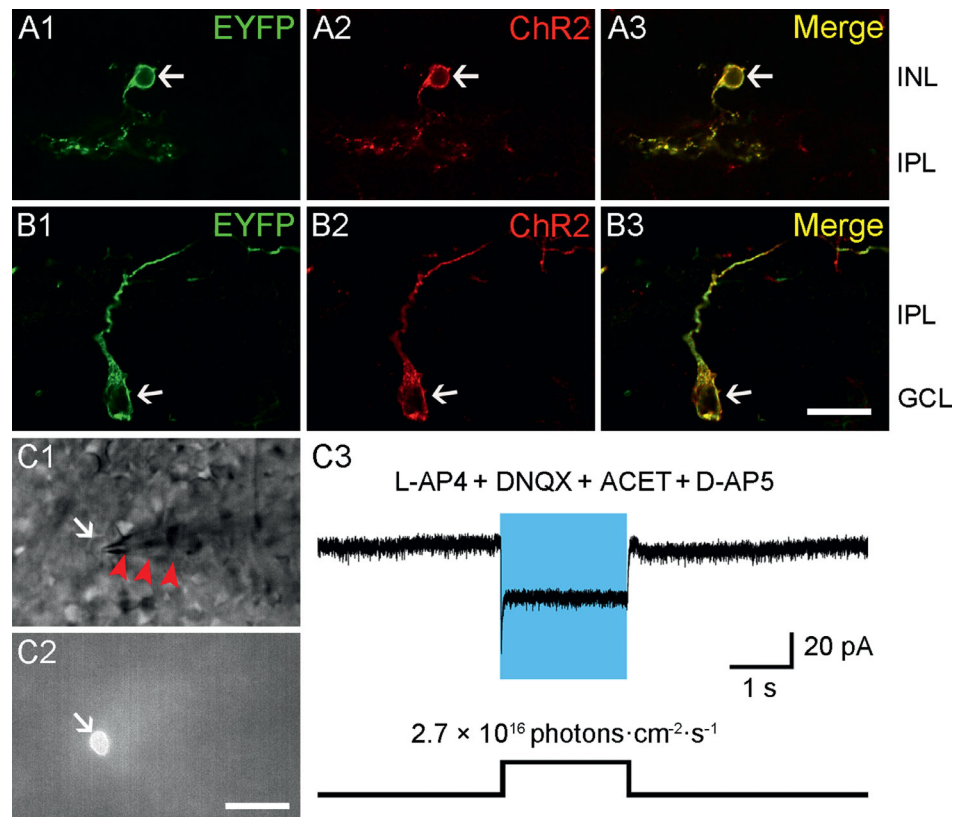
FIGURE 8. Functional ChR2 is expressed by EYFP-positive cells. (**A1−B3**) Confocal photomicrographs of retinal sections co-stained with antibodies recognizing EYFP and ChR2. Robust ChR2 signals are co-localized to EYFP fluorescence in both type I (**A1−A3**) and type II cells (**B1−B3**). Arrows point to somata. Scale bar = 20 μm. (**C1**) Representative infrared image of a whole-mount retina, in which a type I cell (white arrow) was recorded with a micropipette (red arrowheads). (**C2**) A fluorescent image taken in the same area in **C1**, indicating the EYFP-positive soma of the cell recorded. Scale bar = 20 mm. (**C3**) Voltage-clamp recordings of an inward photocurrent (V_{hold}: 67 mV), elicited from the cell shown in **C1** and **C2**, in response to full-field light stimulation in the presence of a glutamatergic blocker cocktail (L-AP4, DNQX, ACET and D-AP5). The blue bar represents the 470 nm light pulse.

may be an ideal model for exploring the physiological functions of nGnG ACs.

Specific Labeling of Brn3b-negative M1 ipRGCs that Project to the SCN

A series of genetic mice probing M1 ipRGCs are now available. The first generated is the Opn4[tau-LacZ] reporter mouse, in which M1 cells are labeled by targeting a gene coding for Tau-lacZ (a fusion protein composed of tau signal peptide and β-galactosidase) into the melanopsin gene locus,[29] thus allowing tracing M1 cell axons down to their central targets.[61] Later, two BAC mice with fluorophores expression driven by the melanopsin promoter[62,63] and one knock-in mouse with Cre expression in melanopsin gene open reading frame[64] were made. These three mice, either along or mated with reporter lines, can be used to visualize not only M1, but also other ipRGC subtypes (M2−M6) in living tissues, thereby facilitating physiological recordings.[32,64−67] Another genetic mouse, the Opn4[CreERT2/+]; Brn3b[CKOAP/+] mouse was generated to achieve inducible alkaline phosphatase staining of Brn3b-expressing ipRGCs, including the Brn3b-expressing M1 cells.[18] To our knowledge, however, there are so far no genetic mice available in which Brn3b-negative M1 cells are specifically labeled. In the retina of the ChAT-ChR2-EYFP mouse, EYFP signals

in the GCL were exclusively localized to Brn3b-negative M1 cells. Thus, this mouse might be the first that enables specific labeling of the second subset of M1 cells which selectively innervate the SCN.

Potential Application in the Future Studies

Ectopic expression of a specific gene generally means that the gene is not expressed in a manner that matches the expected endogenous pattern. It nonetheless might provide serendipitous access to specific neuronal populations and circuits. A recent example comes from the aforementioned ChAT-EGFP mouse in which EGFP is ectopically expressed by multiple subtypes of noncholinergic retinal neurons.[46] Using this mouse, morphological/physiological profiles of a novel wide-field GABAergic AC population (WA-S2/3 cell) were characterized by Knop and colleagues.[49] Similarly, the ChAT-ChR2-EYFP mouse will allow us to target nGnG ACs for exploring their physiological properties and identifying their neurotransmitters, two issues that have not been addressed yet.

Using immunohistochemical double-staining with a ChR2 antibody, we found that ChR2 was indeed expressed in all EYFP-positive cells in the ChAT-ChR2-EYFP retina (Figs. 8A1–B3), thereby confirming the molecular intactness of the ChR2-EYFP fusion protein. Furthermore, whole-cell patch-clamp recordings revealed that EYFP-positive

nGnG ACs were capable of generating light-induced inward currents with current kinetics typical of ChR2-mediated response. These results demonstrated that the expressed ChR2 was well functional (Figs. 8C1–C3). It seems likely that this mouse may be useful for dissecting synaptic connections between nGnG ACs and other retinal neurons by optogenetic manipulation. In fact, such "optogenetic dissections" have been recently conducted on animals with cell-type specific ChR2 targeting to scrutinize neural circuits of various AC subtypes, including VGluT3-containing AC,[15,68,69] VIP-expressing AC,[38] CRH AC,[70] TH2 AC,[71] and SAC.[72]

Specific labeling for Brn3b-negative M1 ipRGCs in the ChAT-ChR2-EYFP retina also provides a good opportunity for determining whether and how the physiological profiles of these cells may be different from those of Brn3b-positive M1 cells and revealing the functional relevance of such difference. Moreover, because the EYFP labeling of M1 cells is limited to the ventral retina, this mouse might be useful in examining the role of topographic organization of the M1-SCN projection in circadian rhythm modulation, when these ventrally located M1 cells are selectively ablated in vivo with immunotoxins recognizing the EYFP protein.[73–75]

References

1. Masland RH. Neuronal diversity in the retina. *Curr Opin Neurobiol*. 2001;11:431–436.

2. Masland RH. The neuronal organization of the retina. *Neuron*. 2012;76:266–280.

3. Baden T, Berens P, Franke K, Roman Roson M, Bethge M, Euler T. The functional diversity of retinal ganglion cells in the mouse. *Nature*. 2016;529:345–350.

4. Bae JA, Mu S, Kim JS, et al. Digital museum of retinal ganglion cells with dense anatomy and physiology. *Cell*. 2018;173:1293–1306e1219.

5. Rheaume BA, Jereen A, Bolisetty M, et al. Single cell transcriptome profiling of retinal ganglion cells identifies cellular subtypes. *Nat Commun*. 2018;9:2759.

6. MacNeil MA, Heussy JK, Dacheux RF, Raviola E, Masland RH. The shapes and numbers of amacrine cells: matching of photofilled with Golgi-stained cells in the rabbit retina and comparison with other mammalian species. *J Comp Neurol*. 1999;413:305–326.

7. MacNeil MA, Masland RH. Extreme diversity among amacrine cells: Implications for function. *Neuron*. 1998;20:971–982.

8. Masland RH. The tasks of amacrine cells. *Vis Neurosci*. 2012;29:3–9.

9. Ivanova E, Hwang GS, Pan ZH. Characterization of transgenic mouse lines expressing Cre recombinase in the retina. *Neuroscience*. 2010;165:233–243.

10. Martersteck EM, Hirokawa KE, Evarts M, et al. Diverse central projection patterns of retinal ganglion cells. *Cell Rep*. 2017;18:2058–2072.

11. Sanes JR, Masland RH. The types of retinal ganglion cells: current status and implications for neuronal classification. *Annu Rev Neurosci*. 2015;38:221–246.

12. Boyden ES. A history of optogenetics: The development of tools for controlling brain circuits with light. *F1000 Biol Rep*. 2011;3:11.

13. Fenno L, Yizhar O, Deisseroth K. The development and application of optogenetics. *Annu Rev Neurosci*. 2011;34:389–412.

14. Miesenbock G. Optogenetic control of cells and circuits. *Annu Rev Cell Dev Biol*. 2011;27:731–758.

15. Lee S, Zhang Y, Chen M, Zhou ZJ. Segregated glycine-glutamate co-transmission from vGluT3 amacrine cells to contrast-suppressed and contrast-enhanced retinal circuits. *Neuron*. 2016;90:27–34.

16. Kay JN, Voinescu PE, Chu MW, Sanes JR. Neurod6 expression defines new retinal amacrine cell subtypes and regulates their fate. *Nat Neurosci*. 2011;14:965–972.

17. Strettoi E, Masland RH. The number of unidentified amacrine cells in the mammalian retina. *Proc Natl Acad Sci U S A*. 1996;93:14906–14911.

18. Chen SK, Badea TC, Hattar S. Photoentrainment and pupillary light reflex are mediated by distinct populations of ipRGCs. *Nature*. 2011;476:92–95.

19. Zhao S, Ting JT, Atallah HE, et al. Cell type-specific channelrhodopsin-2 transgenic mice for optogenetic dissection of neural circuitry function. *Nat Methods*. 2011;8:745–752.

20. Xu GZ, Cui LJ, Liu AL, et al. Transgene is specifically and functionally expressed in retinal inhibitory interneurons in the VGAT-ChR2-EYFP mouse. *Neuroscience*. 2017;363:107–119.

21. Tauchi M, Masland RH. The shape and arrangement of the cholinergic neurons in the rabbit retina. *Proc R Soc Lond B Biol Sci*. 1984;223:101–119.

22. Nadal-Nicolas FM, Jimenez-Lopez M, Sobrado-Calvo P, et al. Brn3a as a marker of retinal ganglion cells: qualitative and quantitative time course studies in naive and optic nerve-injured retinas. *Invest Ophthalmol Vis Sci*. 2009;50:3860–3868.

23. Schlamp CL, Montgomery AD, Mac Nair CE, Schuart C, Willmer DJ, Nickells RW. Evaluation of the percentage of ganglion cells in the ganglion cell layer of the rodent retina. *Mol Vis*. 2013;19:1387–1396.

24. Macosko EZ, Basu A, Satija R, et al. Highly parallel genome-wide expression profiling of individual cells using nanoliter droplets. *Cell*. 2015;161:1202–1214.

25. Shekhar K, Lapan SW, Whitney IE, et al. Comprehensive classification of retinal bipolar neurons by single-cell transcriptomics. *Cell*. 2016;166:1308–1323e1330.

26. Jain V, Ravindran E, Dhingra NK. Differential expression of Brn3 transcription factors in intrinsically photosensitive retinal ganglion cells in mouse. *J Comp Neurol*. 2012;520:742–755.

27. Karnas D, Mordel J, Bonnet D, Pevet P, Hicks D, Meissl H. Heterogeneity of intrinsically photosensitive retinal ganglion cells in the mouse revealed by molecular phenotyping. *J Comp Neurol*. 2013;521:912–932.

28. Berson DM, Castrucci AM, Provencio I. Morphology and mosaics of melanopsin-expressing retinal ganglion cell types in mice. *J Comp Neurol*. 2010;518:2405–2422.

29. Hattar S, Liao HW, Takao M, Berson DM, Yau KW. Melanopsin-containing retinal ganglion cells: architecture, projections, and intrinsic photosensitivity. *Science*. 2002;295:1065–1070.

30. Lin B, Peng EB. Retinal ganglion cells are resistant to photoreceptor loss in retinal degeneration. *PLoS One.* 2013;8:e68084.

31. van der Merwe I, Lukats A, Blahova V, Oosthuizen MK, Bennett NC, Nemec P. The topography of rods, cones and intrinsically photosensitive retinal ganglion cells in the retinas of a nocturnal (Micaelamys namaquensis) and a diurnal (Rhabdomys pumilio) rodent. *PLoS One.* 2018;13:e0202106.

32. Schmidt TM, Kofuji P. Functional and morphological differences among intrinsically photosensitive retinal ganglion cells. *J Neurosci.* 2009;29:476–482.

33. Estevez ME, Fogerson PM, Ilardi MC, et al. Form and function of the M4 cell, an intrinsically photosensitive retinal ganglion cell type contributing to geniculocortical vision. *J Neurosci.* 2012;32:13608–13620.

34. Bina KG, Rusak B, Semba K. Localization of cholinergic neurons in the forebrain and brainstem that project to the suprachiasmatic nucleus of the hypothalamus in rat. *J Comp Neurol.* 1993;335:295–307.

35. Hut RA, Van der Zee EA. The cholinergic system, circadian rhythmicity, and time memory. *Behav Brain Res.* 2011;221:466–480.

36. Wang Y, Lin WK, Crawford W, et al. Optogenetic control of heart rhythm by selective stimulation of cardiomyocytes derived from Pnmt(+) cells in murine heart. *Sci Rep.* 2017;7:40687.

37. Pan ZH, Lu Q, Bi A, Dizhoor AM, Abrams GW. Optogenetic approaches to restoring vision. *Annu Rev Vis Sci.* 2015;1:185–210.

38. Park SJ, Borghuis BG, Rahmani P, Zeng Q, Kim IJ, Demb JB. Function and circuitry of VIP+ interneurons in the mouse retina. *J Neurosci.* 2015;35:10685–10700.

39. Boyden ES, Zhang F, Bamberg E, Nagel G, Deisseroth K. Millisecond-timescale, genetically targeted optical control of neural activity. *Nat Neurosci.* 2005;8:1263–1268.

40. Han Y, Shi YF, Xi W, et al. Selective activation of cholinergic basal forebrain neurons induces immediate sleep-wake transitions. *Curr Biol.* 2014;24:693–698.

41. Ma M, Luo M. Optogenetic activation of basal forebrain cholinergic neurons modulates neuronal excitability and sensory responses in the main olfactory bulb. *J Neurosci.* 2012;32:10105–10116.

42. Ren J, Qin C, Hu F, et al. Habenula "cholinergic" neurons co-release glutamate and acetylcholine and activate postsynaptic neurons via distinct transmission modes. *Neuron.* 2011;69:445–452.

43. Zhang J, Tan L, Ren Y, et al. Presynaptic excitation via GABAB receptors in habenula cholinergic neurons regulates fear memory expression. *Cell.* 2016;166:716–728.

44. Harris JA, Hirokawa KE, Sorensen SA, et al. Anatomical characterization of Cre driver mice for neural circuit mapping and manipulation. *Front Neural Circuits.* 2014;8:76.

45. Korecki AJ, Hickmott JW, Lam SL, et al. Twenty-seven tamoxifen-inducible iCre-driver mouse strains for eye and brain, including seventeen carrying a new inducible-first constitutive-ready allele. *Genetics.* 2019;211:1155–1177.

46. Haverkamp S, Inta D, Monyer H, Wassle H. Expression analysis of green fluorescent protein in retinal neurons of four transgenic mouse lines. *Neuroscience.* 2009;160:126–139.

47. Fuerst PG, Bruce F, Rounds RP, Erskine L, Burgess RW. Cell autonomy of DSCAM function in retinal development. *Dev Biol.* 2012;361:326–337.

48. Lu Q, Ivanova E, Ganjawala TH, Pan ZH. Cre-mediated recombination efficiency and transgene expression patterns of three retinal bipolar cell-expressing Cre transgenic mouse lines. *Mol Vis.* 2013;19:1310–1320.

49. Knop GC, Pottek M, Monyer H, Weiler R, Dedek K. Morphological and physiological properties of enhanced green

fluorescent protein (EGFP)-expressing wide-field amacrine cells in the ChAT-EGFP mouse line. *Eur J Neurosci.* 2014;39:800–810.

50. Zhu Y, Xu J, Hauswirth WW, DeVries SH. Genetically targeted binary labeling of retinal neurons. *J Neurosci.* 2014;34:7845–7861.

51. Vuong HE, Perez de Sevilla Muller L, Hardi CN, McMahon DG, Brecha NC. Heterogeneous transgene expression in the retinas of the TH-RFP, TH-Cre, TH-BAC-Cre and DAT-Cre mouse lines. *Neuroscience.* 2015;307:319–337.

52. Gabriel R, Erdelyi F, Szabo G, Lawrence JJ, Wilhelm M. Ectopic transgene expression in the retina of four transgenic mouse lines. *Brain Struct Funct.* 2016;221:3729–3741.

53. Gong S, Doughty M, Harbaugh CR, et al. Targeting Cre recombinase to specific neuron populations with bacterial artificial chromosome constructs. *J Neurosci.* 2007;27:9817–9823.

54. Gong S, Yang XW, Li C, Heintz N. Highly efficient modification of bacterial artificial chromosomes (BACs) using novel shuttle vectors containing the R6Kgamma origin of replication. *Genome Res.* 2002;12:1992–1998.

55. Gelman DM, Noain D, Avale ME, Otero V, Low MJ, Rubinstein M. Transgenic mice engineered to target Cre/loxP-mediated DNA recombination into catecholaminergic neurons. *Genesis.* 2003;36:196–202.

56. Jeon CJ, Strettoi E, Masland RH. The major cell populations of the mouse retina. *J Neurosci.* 1998;18:8936–8946.

57. Chew KS, Renna JM, McNeill DS, et al. A subset of ipRGCs regulates both maturation of the circadian clock and segregation of retinogeniculate projections in mice. *Elife.* 2017;6:pii: e22861.

58. Marquardt T, Ashery-Padan R, Andrejewski N, Scardigli R, Guillemot F, Gruss P. Pax6 is required for the multipotent state of retinal progenitor cells. *Cell.* 2001;105:43–55.

59. Cherry TJ, Trimarchi JM, Stadler MB, Cepko CL. Development and diversification of retinal amacrine interneurons at single cell resolution. *Proc Natl Acad Sci U S A.* 2009;106:9495–9500.

60. Voinescu PE, Kay JN, Sanes JR. Birthdays of retinal amacrine cell subtypes are systematically related to their molecular identity and soma position. *J Comp Neurol.* 2009;517:737–750.

61. Hattar S, Kumar M, Park A, et al. Central projections of melanopsin-expressing retinal ganglion cells in the mouse. *J Comp Neurol.* 2006;497:326–349.

62. Do MT, Kang SH, Xue T, et al. Photon capture and signalling by melanopsin retinal ganglion cells. *Nature.* 2009;457:281–287.

63. Schmidt TM, Taniguchi K, Kofuji P. Intrinsic and extrinsic light responses in melanopsin-expressing ganglion cells during mouse development. *J Neurophysiol.* 2008;100:371–384.

64. Ecker JL, Dumitrescu ON, Wong KY, et al. Melanopsin-expressing retinal ganglion-cell photoreceptors: cellular diversity and role in pattern vision. *Neuron.* 2010;67:49–60.

65. Quattrochi LE, Stabio ME, Kim I, et al. The M6 cell: A small-field bistratified photosensitive retinal ganglion cell. *J Comp Neurol.* 2019;527:297–311.

66. Schmidt TM, Kofuji P. Structure and function of bistratified intrinsically photosensitive retinal ganglion cells in the mouse. *J Comp Neurol.* 2011;519:1492–1504.

67. Stabio ME, Sabbah S, Quattrochi LE, et al. The M5 cell: A color-opponent intrinsically photosensitive retinal ganglion cell. *Neuron.* 2018;97:150–163e154.

68. Lee S, Chen L, Chen M, Ye M, Seal RP, Zhou ZJ. An unconventional glutamatergic circuit in the retina formed by vGluT3 amacrine cells. *Neuron.* 2014;84:708–715.

69. Tien NW, Kim T, Kerschensteiner D. Target-specific glycinergic transmission from VGluT3-expressing amacrine cells shapes suppressive contrast responses in the retina. *Cell Rep*. 2016;15:1369–1375.

70. Park SJH, Pottackal J, Ke JB, et al. Convergence and divergence of CRH amacrine cells in mouse retinal circuitry. *J Neurosci*. 2018;38:3753–3766.

71. Kim T, Kerschensteiner D. Inhibitory control of feature selectivity in an object motion sensitive circuit of the retina. *Cell Rep*. 2017;19:1343–1350.

72. Yonehara K, Balint K, Noda M, Nagel G, Bamberg E, Roska B. Spatially asymmetric reorganization of inhibition establishes a motion-sensitive circuit. *Nature*. 2011;469:407–410.

73. Antonucci F, Alpar A, Kacza J, et al. Cracking down on inhibition: Selective removal of GABAergic interneurons from hippocampal networks. *J Neurosci*. 2012;32:1989–2001.

74. Goz D, Studholme K, Lappi DA, Rollag MD, Provencio I, Morin LP. Targeted destruction of photosensitive retinal ganglion cells with a saporin conjugate alters the effects of light on mouse circadian rhythms. *PLoS One*. 2008;3:e3153.

75. Yoshida K, Watanabe D, Ishikane H, Tachibana M, Pastan I, Nakanishi S. A key role of starburst amacrine cells in originating retinal directional selectivity and optokinetic eye movement. *Neuron*. 2001;30:771–780.